Localised Measurements of pH and Dissolved Oxygen as Complements to SVET in the Investigation of Corrosion at Defects in Coated Aluminum Alloy

A. C. Bastos, O. V. Karavai, M. L. Zheludkevich, K. A. Yasakau, M. G. S. Ferreira*

DECV/CICECO, Universidade de Aveiro, 3810-193 Aveiro, Portugal
*acbastos@ua.pt

Received: January 29, 2010
Accepted: March 8, 2010

Abstract
This paper presents measurements of local pH and local oxygen reduction current performed to complement SVET (Scanning Vibrating Electrode Technique) in the characterization of the chemical environment near artificial defects on coated 2024-T3 aluminum alloy during corrosion and inhibition. The main purpose is to give examples on how micropotentiometry and microamperometry can add supplementary information to SVET, providing important insights for the understanding of corrosion mechanisms and inhibition processes necessary to develop effective self-healing coatings.

Keywords: Corrosion, Microelectrodes, Oxygen reduction, pH, SVET

DOI: 10.1002/elan.201000076

Presented at the International Conference on Modern Electroanalytical Methods Prague, December 9–14, 2009

1. Introduction

Application of protective organic coatings is the most widespread anticorrosive method due to low cost, versatility and simple application [1, 2]. Frequently, the degradation of coated metals begins in small areas where the metallic substrate becomes exposed, either due to improper paint application (e.g. pinholes) or by later damage (e.g. scratches) [1, 3]. It is important to understand the mechanisms of corrosion in these confined areas and how inhibitors that may be added to the coatings can retard the corrosion progression. The majority of the techniques give the average response of the whole sample area, overlooking the difference in reactivity at the defects and at the remaining area.

The spatial distribution of the corrosion processes can be obtained by localized techniques. The application of SECM (Scanning Electrochemical Microscopy) with micro- and nanoelectrodes for localized electrochemical studies has been recently reviewed [4]. In the case of coated metallic substrates, SECM operating in AC mode allows the identification of the areas with higher conductivity, resulting from the increased concentration of ionic species near the active defects. This method is rather qualitative and can be used only in low-conductivity solutions [5], which hardly is the case of corrosive aqueous environments. Another technique, the Scanning Vibrating Electrode Technique (SVET), detects the potential gradients that develop around anodic and cathodic areas as a consequence of current flow [6, 7]. It makes possible to know the spatial evolution of cathodic and anodic processes in a corroding sample. This information is unique and extremely useful for the description of many corrosion systems. The technique is only sensitive to charged species and doesn't give the identity of the species detected. Such identification can be done using potentiometric [8–12] and amperometric [13–16] microelectrodes.

In this paper, micropotentiometric measurements of pH and microamperometric measurements of dissolved oxygen were used as complements to SVET in the investigation of corrosion and inhibition of coated 2024-T3 aluminum alloy with artificial defects. The samples were immersed in 0.05 M NaCl and measurements were performed before and after the addition of a corrosion inhibitor (cerium nitrate) to the solution. The objective was to simulate the release of the inhibitor (it was added directly to solution instead of the slow leaching from the coating) and check the potential of these techniques to study the kinetics of corrosion and inhibition processes. Ultimately, the idea is to verify their ability to probe self-healing properties of new coatings, which is, these days, a hot topic in the protective coatings field [17, 18]. Here, only two species were probed. A better, more complete, picture would be obtained if more species were measured.

2. Experimental

2.1. Samples

Metal plates of 2024-T3 aluminum alloy were coated with a dense 2 μm thick hybrid organic-inorganic film. The film was synthesized via the sol-gel route, mixing two different sols, one prepared by acid catalysed hydrolysis of zirconium(IV) propoxide (70 wt.% in 2-propanol) and ethylacetoacetate (1:1 volume ratio) and another sol prepared by acid catalysed hydrolysis of (3-glycidoxypropyl)-trimethoxysilane and 2-propanol (1:1 volume ratio). The final sol–gel solution (with 1:2 volume ratio of the first and the second sol, respectively) was stirred under ultrasonic agitation for 1 h and aged for 1 h. More details on the synthesis can be found in [19].

The AA2024-T3 samples were etched using an industrial 3-step cleaning procedure: (1) alkaline cleaning in 48 ± 2 g L^{-1} Metaclean T2001 (CVH Chemie-Vertrieb GmbH & Co. Hannover KG, Germany) at $65 \pm 5\,^{\circ}C$ for 20 ± 5 min, followed by (2) alkaline etching in 65 ± 5 g L^{-1} Turco Liquid Aluminetch N2 (Henkel, Germany) at $60 \pm 5\,^{\circ}C$ for 45 ± 15 s and completed by (3) acid etching in 180 ± 10 mL L^{-1} Turco Liquid Smutgo NC (Henkel, Germany) at $25 \pm 7\,^{\circ}C$ for 8 ± 2 min. The samples were thoroughly washed in distilled water between each cleaning step. At the end they were dried in a flow of warm air.

The metal substrates were immersed in the mixed sol solution during 100 seconds and removed at a speed of 18 cm min^{-1}, using a home-made dip-coater with vibration isolation. Solvent evaporation, gelation and cross-linking took place in an oven at 120 °C during 80 min. Pieces of 1×1 cm^2 were cut and glued to epoxy sample holders and the edges protected with beeswax + colophony (3:1 wt. ratio). Scotch tape around the epoxy holders provided the solution reservoir. Round-shaped defects down to the metal substrate with an approximate diameter of 150 μm and separated by 300 μm were produced with a sharp needle (Figure 1). The corrosive environment was 0.05 M NaCl made with distilled water and p.a. grade reagent. The medium was made inhibitive by addition of crystals of $Ce(NO_3)_3 \cdot 6H_2O$ (Aldrich, p.a.) to the solution until reaching a concentration of 10 mM in Ce^{3+}. The pH and dissolved O_2 concentration of the two solutions were determined at 23.0 °C with a Hach-Lange HQ40d Multi with a PHC301 electrode for pH and a LDO101 electrode for O_2 (using the luminescence method). The pH was 6.0 ± 0.2 for 0.05 M NaCl and 5.7 ± 0.2 for 0.05 M NaCl + 0.01 M $Ce(NO_3)_3$. The concentration of dissolved O_2 in both solutions was found to be within $2.5 \pm 0.1 \times 10^{-4}$ M.

2.2. SVET

The SVET equipment was manufactured by Applicable Electronics Inc. (USA) and controlled by the ASET 2.0 program developed by Sciencewares (USA). The SVET microelectrode was prepared from polymer insulated Pt-Ir

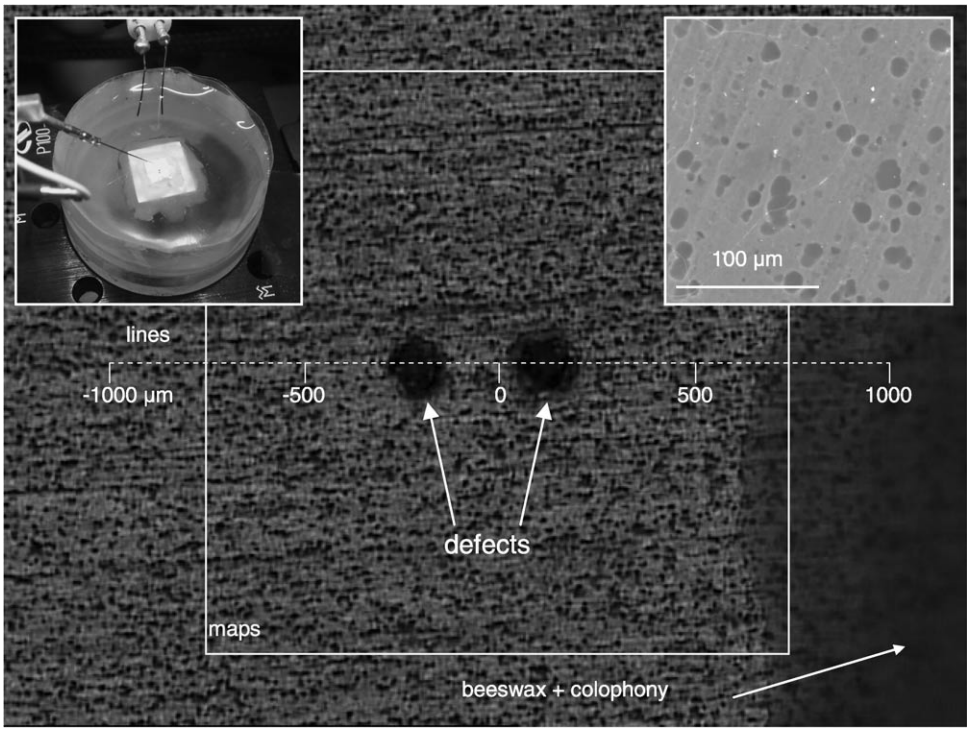

Fig. 1. Sample's surface with indication of the two artificial defects and the position of maps and lines. The myriad of dark spots scattered throughout the surface is a result of the cleaning process that removed the intermetallic precipitates at the surface leaving small holes, later filled by the sol-gel film. Left inset is a sample in the epoxy holder during a SVET measurement. Right inset is a detail of the small holes filled by the sol-gel film.

microelectrodes produced by Microprobes Inc. (USA). A 10 – 20 μm diameter platinum black sphere was electrodeposited on the tip. While it's possible to vibrate the microelectrode in two directions, one parallel (x axis) and another normal (z axis) to the sample's surface, only signals from the normal field were considered in the present study. The frequency was 162 Hz and the amplitude of vibration was two times the tip diameter. The measured potential differences were converted to ionic currents after a calibration routine performed with a point current source (microelectrode with a tip of ~3 μm) driving a current of 60 nA at 150 μm from the vibrating probe [20 – 22]. The calibration is valid for a new solution provided the system is updated with its resistivity. The maps and lines were obtained at a plane 100 μm above the sample's surface.

2.3. Micropotentiometry

The pH micropotentiometric electrodes were made in the laboratory. Single-barrelled borosilicate glass capillaries with an outer diameter of 1.5 mm (WPI, USA, Ref. TW150-4) were thinned with a P97 micropipette puller (Sutter, USA) using a four step pulling protocol giving a tip of 2 μm in diameter on one end. The micropipettes were silanized for 2 hours in an oven at 200 °C after injection of 200 μL of *N,N*-dimethyltrimethylsilylamine (Fluka, Ref. 41716). The micropipette was back-filled with 0.1 M $KCl + KH_2PO_4$ 0.01 M – internal solution – to a length of 5 mm from the tip and front-filled with a 20 – 30 μm column of hydrogen I cocktail B ionophore (Fluka, Ref. 95293). It was then inserted in a half-cell plastic holder (WPI, USA, Ref. EHB1) containing a chloridised silver wire as internal reference electrode. A homemade Ag | AgCl, 0.05 M NaCl electrode worked as external reference electrode. The microelectrode was mounted in the same 3D positioning system used for SVET. A IPA2 amplifier (input resistance $>10^{15}$ Ω) manufactured by Applicable Electronics Inc. was controlled by the ASET program to measure and record the data. The microelectrodes were calibrated before and after measurements with commercial pH buffers (Riedel-de Haen), giving a linear response in the 5 to 13 pH range (Figure 2).

2.4. Microamperometry

The microamperometric detection of dissolved oxygen was based on the reaction

$$2H_2O(l) + O_2(g) + 4e^- \rightarrow 4OH^-(aq) \quad (1)$$

and was performed using the IPA2 amplifier in the amperometric mode. A two electrode arrangement was used, with a 10 μm diameter platinum microdisk (CH Instruments, USA, Ref. CHI100) as working electrode (sensor) and a homemade Ag | AgCl electrode as counter/reference electrode. Given the small currents to be measured (pico to nano amperes) this electrode can maintain its integrity and a fairly stable potential, especially if the measurements are not too long. The tip potential was set at – 0.7 V vs. Ag | AgCl, well inside the region where oxygen reduction current was diffusion controlled (Figure 3). The electrode and the preamplifier were mounted in the same 3D positioning system used for SVET and the ASET program controlled the measurements.

3. Results and Discussion

In all experiments the metal substrate was exposed to solution just in the two artificial defects. The remaining metal surface was protected by the hybrid organic-inorganic sol-gel film and by insulating beeswax + colophony. The sol-gel coating provided an efficient barrier to the environment and prevented corrosion in non damaged areas. The SVET

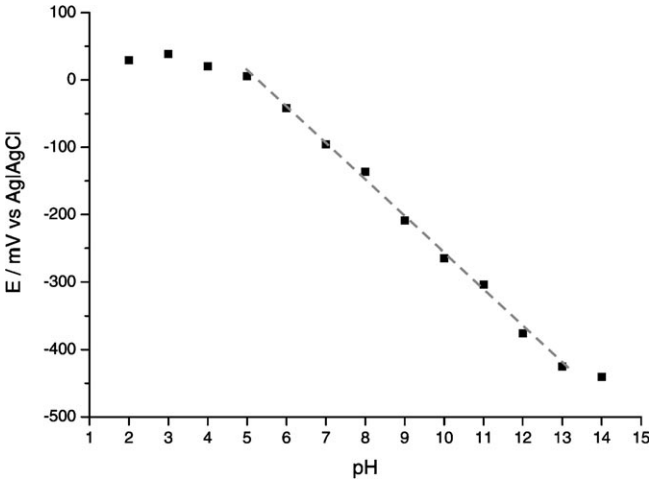

Fig. 2. Potentiometric response of the pH microelectrode with commercial pH buffers. Slope = – 54.45 mV/pH unit.

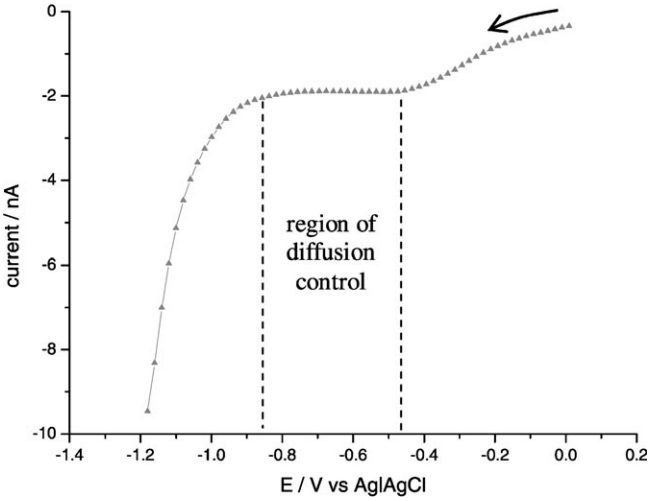

Fig. 3. Voltammogram recorded with the platinum microelectrode immersed in 0.05 M NaCl, depicting the waves for the diffusion limited oxygen reduction and the reduction of water. Scan rate: 30 mV s^{-1}.

map presented in Figure 4a shows negative currents on the left defect and positive currents on the right defect. The positive currents are associated with an upward net flux of cations produced by the anodic process and negative currents are associated with an upward net flux of anions originated from the cathodic processes. The anodic activity can be attributed mainly to the dissolution of aluminum from the alloy matrix, and dissolution of Mg and Al from S-phase intermetallics (Al_2CuMg) according to the reaction,

$$M(s) \rightarrow M^{n+}(aq) + ne^- \quad (2)$$

where M^{n+} is Al^{3+} or Mg^{2+}.

In the case of the cathodic process, two reactions are possible: the hydrogen evolution,

$$2H^+(aq) + 2e^- \rightarrow H_2(g) \quad (3)$$

and the reduction of dissolved oxygen, reaction (1). Both reactions lead to local alkalization.

SVET detected the corrosion activity 2 hours after immersion, initially as very small currents that increased in magnitude with time until a steady value. The map of Figure 4a was obtained after 19 hours of immersion in 0.05 M NaCl. The anodic and cathodic regions stayed in the same position since the beginning. After this measurement cerium nitrate was added to solution in order to estimate its inhibition capability. Figure 4b shows the current map measured 19 hours after the addition of cerium nitrate. No activity was detected then. This means the inhibitor successfully stopped the corrosion process at the defects. The corrosion inhibition by cerium nitrate is attributed to the blocking of the cathodic process by precipitation of cerium hydroxide in the cathodic sites [23–26],

$$Ce^{3+}(aq) + 3OH^-(aq) \rightarrow Ce(OH)_3(s) \downarrow \quad (4)$$

Cerium oxides, namely CeO_2 and Ce_2O_3, may be formed as well [24–26]. Once the original cathodic sites become blocked, the anodic and cathodic reactions will take place in the area still active. The blocking of the new cathodic sites reduces even more the active area and the process continues until all area becomes covered.

The kinetics of inhibition of corrosion processes in microconfined defects can be followed by SVET. This is important for estimating the effectiveness of corrosion inhibitors to be used in self-healing coatings. Figure 5 shows SVET scan lines obtained 100 μm above the defects at selected times after addition of crystals of cerium nitrate to solution. The corrosion activity was already lower just 3 minutes after the addition of inhibitor and kept falling in the subsequent hours.

Considering that the currents measured in solution by SVET are related to the active metal area, which becomes smaller with time by the action of the inhibitor, Equation 5 can be used to estimate the fraction of covered area, θ,

$$\theta = 1 - (i/i_0) \quad (5)$$

where i_0 is the current density before addition of inhibitor and i is the current density after inhibitor.

This equation is usually applied with organic corrosion inhibitors that reduce the active area by adsorbing on the metal surface [27]. Here, the active area is reduced by precipitation of an inorganic layer. Figure 6 gives the evolution of covered area in the hours that follow the addition of inhibitor, calculated from Equation 5 and using the peak currents measured above the right and left defects. Following a fast increase in the first minutes, the covered area continued enlarging until it became completely covered at about 12 hours.

Results presented so far showed the suitability of SVET to study the self-healing of microdefects in protective coatings applied on metallic surfaces. Alone, this technique can give a very good picture of the localized processes taking place over time. Still, more can be obtained. In order to get additional information on the local chemical environment in the corroding sites, micropotentiometry was used to mea-

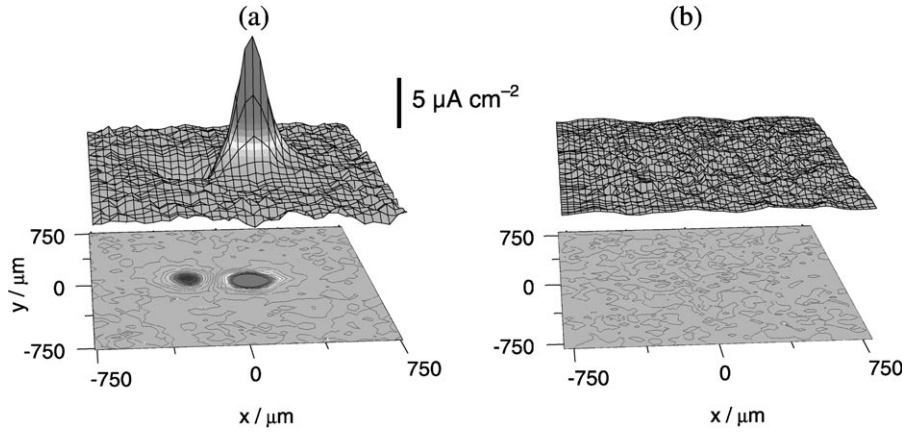

Fig. 4. (a) SVET map obtained 19 h after immersion in 0.05 M NaCl and minutes before the addition of cerium nitrate (corrosion inhibitor); (b) SVET map obtained 19 h after the addition of cerium nitrate to the solution until a concentration of 10 mM. Maps position is indicated in Figure 1.

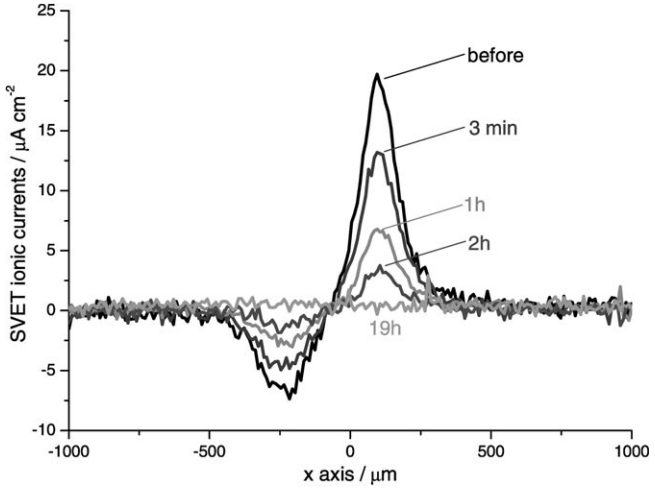

Fig. 5. (a) SVET line scans obtained during the first 19 h after the addition of cerium nitrate. Lines position is indicated in Figure 1.

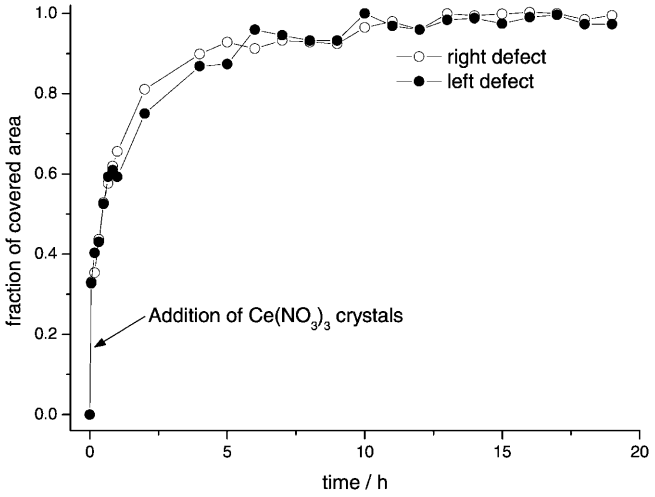

Fig. 6. Fraction of covered metal area calculated with Equation 5 using the maximum values of the right and left peaks.

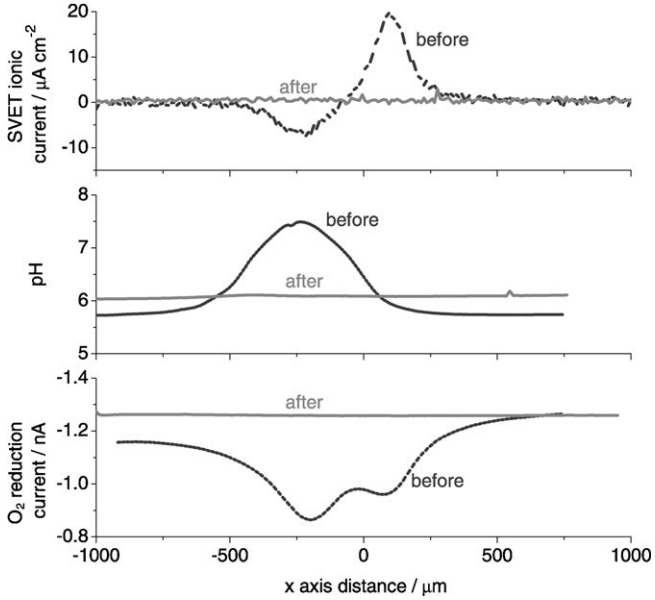

Fig. 7. Line scans of ionic currents (SVET), pH and dissolved oxygen reduction current, obtained at 50 μm (100 μm for SVET) above the surface, before and 20 h after addition of cerium nitrate to the solution. Lines position is indicated in Figure 1.

sure local variations of pH and microamperometry was used to probe the distribution of dissolved oxygen in solution. Figure 7 shows the variation of ionic currents, pH and the reduction current of dissolved oxygen in lines above the artificial defects at a constant height from the surface immediately before and after 20 hours of inhibitor addition. The height was 50 μm for pH and O_2 measurements and 100 μm for SVET. SVET lines show the negative and positive currents above the cathodic and anodic defects, respectively. The pH in solution had a significant increase close to the cathode and no variation was detected above the anode. The measured current due to oxygen reduction (negative by definition) was constant except at positions near both defects where it was smaller. In the inhibited medium the three quantities, ionic currents, local pH and O_2 reduction current, showed the same values encountered in the bulk solution; no local changes existed, confirming that the corrosion process was halted by the inhibitor.

Figure 8 shows the three quantities measured over each of the two defects, following approach curves along the z axis, before and after the addition of inhibitor. The minimum height probed was 50 μm for pH and O_2, and 100 μm for SVET. It was observed the same tendency as before: in the uninhibited medium, SVET showed positive currents above the right defect and negative currents above the left defect, pH increased in the left defect and oxygen current decreased close to both defects. Values changed with the distance to the surface but above 300 – 400 μm they became constant and similar to those in the bulk solution. 20 hours after addition of inhibitor the measured values were constant, regardless the position of measurement and the distance to the surface.

The measurements of pH presented in Figures 7 and 8 show an increase in the left defect, consistent with cathodic activity and with an upward flux of hydroxyl ions detected as negative currents by SVET. Reactions 1 and 3 can be responsible for the local alkalization. The microamperometric measurement of local oxygen distribution was used to clarify the cathodic process. The decrease of reduction current measured near the defects means less oxygen to react at the microdisk due to its consumption to "feed" Reaction 1 at the defects. The confirmation of Reaction 1 does not discard Reaction 3 but, given the pH of the exposure solution (~6) and being the corrosion potential close to −0.6 V vs. Ag | AgCl, its contribution should be negligible. Besides, no hydrogen evolution was observed in the cathodic defect.

Surprisingly, oxygen depletion was detected on the anodic defect as well. The drop of oxygen concentration in the two defects contradicts the initial assumption given by SVET of a

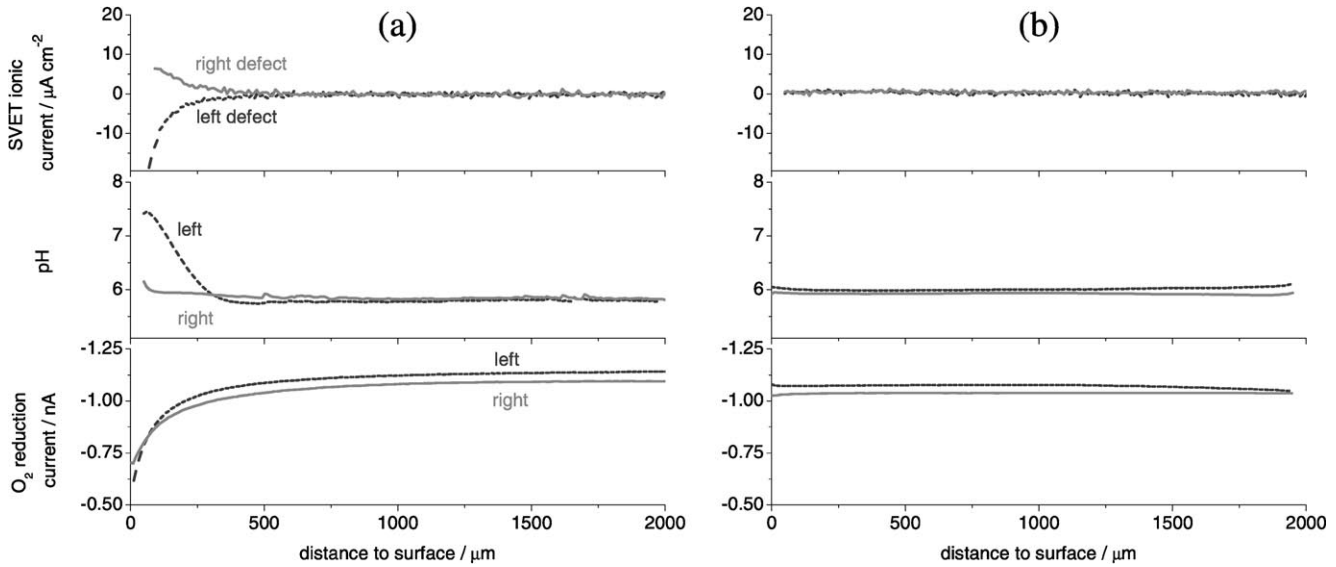

Fig. 8. Ionic currents (SVET), pH and O_2 reduction current measured in the z direction above the two defects before and 20 h after the addition of cerium nitrate.

sole cathode and a sole anode. In fact, one defect is predominantly cathodic and the other is predominantly anodic but cathodic activity exists in both, since the metal substrate is at a potential around -0.6 V vs. Ag | AgCl, potential where oxygen can be reduced. This shows the importance of complementing SVET with other techniques. Given that SVET measures the net response, a small anodic current could also exist in the left defect, being masked by a larger cathodic current. The detection of Al^{3+} in solution would provide that extra information but this is not yet achievable. The potentiometric measurement of Mg^{2+} with a microelectrode [28] was attempted but its detection was unsuccessful. This means that either oxidation isn't occurring on the left defect or, if it is taking place, it generates Mg^{2+} in an amount lower than the detection limit.

The method used in this work to measure dissolved oxygen has some experimental limitations. Application of the equation for the diffusion controlled limiting current at a microdisk [29]

$$i_{L,O2} = 4\, n\, F\, D_{O2}\, C_{O2}\, r \qquad (6)$$

with n being the number of electrons transferred during the oxygen reduction reaction (assumed to be 4), F the Faraday constant, D_{O2} the dissolved oxygen diffusion coefficient in water (2.01×10^{-9} m^2 s^{-1} [30]), C_{O2} the dissolved oxygen concentration in 0.05 M NaCl ($2.5 \pm 0.1 \times 10^{-4}$ M, experimental, or 2.6×10^{-4} M, taken from literature [31]) and r the microdisk radius (5 µm), gives a value of 4 nA. The limiting current measured in this work was 1 to 1.25 nA. Even taking into account that the true n may be less than 4 (apparent values of 2.64 and 2.8 were found in practice [32]) the experimental value is still too low. Reasons for the discrepancy may be a tip radius smaller than the one considered in the calculation and the possibility of side oxidation reactions that, occurring at the same tip potential, would decrease the current measured by the system. Another reason is the poisoning of the platinum surface by impurities that decreases the active area and can lead to its deactivation at long timescales. The possibility of $Al(OH)_3$ precipitation exists when the tip, with local high pH due to reaction (1), passes close to the anodic sites (sources of Al^{3+}). This poisoning problem is usually solved through the use of oxygen semi-permeable membranes [31, 33] or by periodically cleaning the electrode by cycling the tip potential between the oxygen and hydrogen evolution [32, 34]. In this work cycles between -2 and $+1.5$ V vs. Ag | AgCl were produced after each line.

An extreme case of tip deactivation was observed in the presence of Ce^{3+}. Figure 9 shows the result of an experiment where the probe was immersed in 0.05 M NaCl and crystals of cerium nitrate were added to the solution until a concentration of 10 mM in Ce^{3+}. The drop of current is attributed to the precipitation of cerium hydroxide at the tip (Reaction 4) which dramatically reduces the active electrode area, thus diminishing the measured current. Hence, the amperometric detection of O_2 was not possible in the inhibitive solution. For this reason the measurement of dissolved oxygen in Figures 7 and 8 was done after replacing the inhibitive solution with fresh 0.05 M NaCl. Repeating the measurement 24 hours after replacement the values were still the same; the metal in the defects was still protected by the inhibitor layer believed to be formed on its surface.

4. Conclusions

In this work the corrosion at defects on coated AA2024-T3 was investigated from the solution side. Ionic currents measured by SVET permitted to follow the evolution of the anodic and cathodic processes and were complemented with

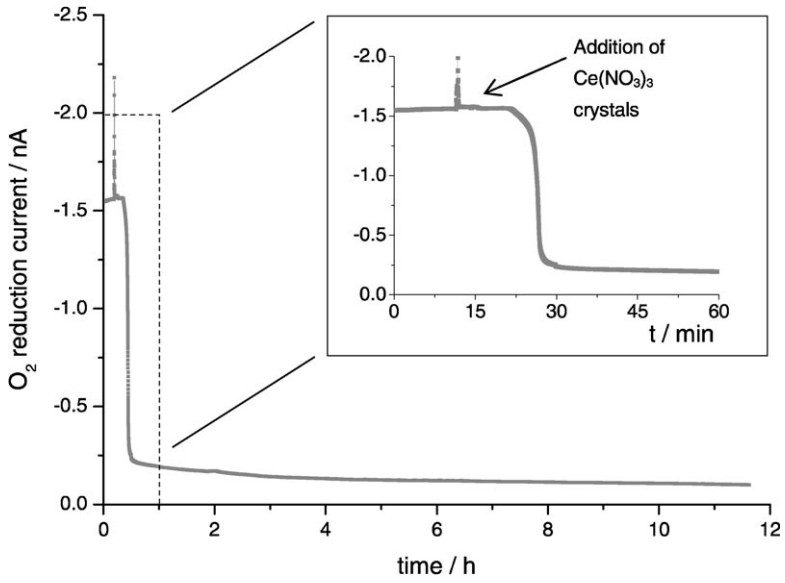

Fig. 9. Chronoamperometric response of the platinum microelectrode immersed in 0.05 M NaCl + 0.01 M $Ce(NO_3)_3$ and polarized at −0.7 V vs. Ag | AgCl.

localized measurements of pH and O_2 reduction current. It was found cathodic activity in a defect that was thought to be only anodic according to SVET data, demonstrating the importance of complement its information with other techniques.

SVET can be used to investigate the kinetics of corrosion and corrosion inhibition at defects of coated metals. Together with micropotentiometric and microamperometric measurements it can give valuable information to disclose the mechanisms of these processes which is an issue of primary importance to develop self-healing anticorrosive coatings.

Acknowledgements

The authors thank Prof. *J. G. Kunkel* (Department of Biology, University of Massachusetts, USA) for the micropipette pulling protocol. *FCT* (Portugal) is acknowledged for a post-doc grant (A. C. Bastos) and two PhD grants (O. V. Karavai and K. A. Yasakau). Financial support from Projects REEQ/719/CTM/2005-*Ecofuels*, PTDC/CTM/66041/2006 and PTDC/CTM/65632/2006 (*FCT*, Portugal) is also acknowledged.

References

[1] C. G. Munger, *Corrosion Prevention by Protective Coatings*, National Association of Corrosion Engineers, Houston, TX **1984**.
[2] Z. W. Wicks Jr., F. N. Jones, S. P. Pappas, *Organic Coatings: Science and Technology* 2nd ed., Wiley, New York **1999**.
[3] *Corrosion Control by Organic Coatings* (Ed: H. Leidheiser Jr.), National Association of Corrosion Engineers, Houston, TX **1981**.
[4] G. Wittock, M. Burchardt, S. E. Pust, Y. Shen, C. Zhao, *Angew. Chem.: Int. Ed.* **2007**, *46*, 1584.
[5] B. Ballesteros Katemann, C. G. Inchauspe, P. A. Castro, A. Schulte, E. J. Calvo, W. Schuhmann, *Electrochim. Acta* **2003**, *48*, 1115.
[6] H. S. Isaacs, Y. Ishikawa, in *Electrochemical Techniques for Corrosion Enginnering* (Ed: R. Baboian), National Association of Corrosion Engineers, Houston, TX **1986**, p. 17.
[7] H. S. Isaacs, *Corros. Sci.* **1988**, *28*, 547.
[8] D. Ammann, *Ion-Selective Micro-electrodes, Principles, Design and Application*, Springer-Verlag, Berlin **1986**.
[9] E. Klusmann, J. W. Schultze, *Electrochim. Acta* **1997**, *42*, 3123.
[10] K. Ogle, V. Baudu, L. Garrides, X. Philippe, *J. Electrochem. Soc.* **2000**, *147*, 3654.
[11] E. Tada, K. Sugawara, H. Kaneko, *Electrochim. Acta* **2004**, *49*, 1019.
[12] H. Ding, L. H. Hihara, *J. Electrochem. Soc.* **2005**, *152*, B161.
[13] *Microelectrodes: Theory and Applications* (Eds: M. Irene Montenegro, M. Arlete Queirós, J. L. Daschbach), NATO Science Series E, Vol. 197, Kluwer Academic Press, Dordrecht, The Netherlands **1991**.
[14] N. Casillas, S. J. Charlebois, W. S. Smyrl, H. S. White, *J. Electrochem. Soc.* **1993**, *140*, L142.
[15] E. Tada, S. Satoh, H. Kaneko, *Electrochim. Acta* **2004**, *49*, 2279.
[16] E. Volker, C. G. Inchauspe, E. J. Calvo, *Electrochem. Commun.* **2006**, *8*, 179.
[17] M. Zheludkevich, "Self-healing Anticorrosion Coatings", in *Self-Healing Materials, Fundamentals, Design Strategies, and Applications* (Ed: S. K. Ghosh), Wiley-VCH, Weinheim, **2008**.
[18] *Self-Healing Properties of New Surface Treatments*, European Federation of Corrosion Series Vol. 58, Maney Publishing **2010**.
[19] S. V. Lamaka, M. L. Zheludkevich, K. A. Yasakau, R. Serra, S. K. Pozniak, M. G. S. Ferreira, *Prog. Org. Coat.* **2007**, *58*, 127.
[20] A. C. Bastos, A. M. Simões, M. G. Ferreira, *Port. Electrochim. Acta* **2003**, *21*, 371.

[21] C. Scheffey, in *Ionic Currents in Development* (Ed: R. Nucitelli), Alan Liss, New York **1986**, p. xxv.
[22] C. Scheffey, *Rev. Sci. Instrum.* **1988**, *59*, 787.
[23] B. R. W. Hinton, *Metals Forum* **1984**, *7*, 211.
[24] A. J. Aldykewicz Jr., H. S. Isaacs, A. J. Davenport, *J. Electrochem. Soc.* **1995**, *142*, 3342.
[25] A. J. Aldykiewicz Jr., A. J. Davenport, H. S. Isaacs, *J. Electrochem. Soc.* **1996**, *143*, 147.
[26] K. Aramaki, *Corros. Sci.* **2001**, *43*, 1573.
[27] C*orrosion*, Vol. 2, 3rd ed. (Eds: Shreir, Jarman, Burstein), Butterworth Heinemann, Oxford **2000**, pp. 20 – 27.
[28] S. V. Lamaka, O. V. Karavai, A. C. Bastos, M. L. Zheludkevich, M. G. S. Ferreira, *Electrochem. Commun.* **2008**, *10*, 259.
[29] A. J. Bard, F.-R. Fan, M. V. Mirkin, in *Physical Electrochemistry: Principles, Methods and Applications* (Ed: I. Rubinstein), Marcel Dekker, New York **1995**, p. 209.
[30] *Handbook of Chemistry and Physics*, 84th ed. (Ed: David R. Lide), CRC Press, Boca Raton, Florida **2003**.
[31] M. L. Hitchman, *Measurement of Dissolved Oxygen*, Wiley, New York, **1978**, p. 22.
[32] M. Sosna, G. Denuault, R. W. Pascal, R. D. Prien, M. Mowlem, *Sens. Actuators B* **2007**, *123*.
[33] I. Fatt, *Polarographic Oxygen Sensors. Its Application in Biology, Medicine, and Technology*, CRC Press, Boca Raton, Florida **1976**.
[34] D. Pletcher, S. Sotiropoulos, *Anal. Chim. Acta* **1996**, *322*, 83.

